arXiv:astro-ph/0212091 v1 4 Dec 2002

VLBA CONTINUUM AND H I ABSORPTION OBSERVATIONS OF THE ULTRA-LUMINOUS INFRARED GALAXY IRAS 17208–0014

Emmanuel Momjian[1,2]

momjian@pa.uky.edu

Jonathan D. Romney[1]

jromney@nrao.edu

Christopher L. Carilli[1]

ccarilli@nrao.edu

Thomas H. Troland[2]

troland@pa.uky.edu

and

Gregory B. Taylor[1]

gtaylor@nrao.edu

ABSTRACT

We present phase-referenced VLBI observations of the radio continuum emission from, and the neutral hydrogen 21 cm absorption toward, the Ultra-Luminous Infrared Galaxy IRAS 17208–0014. The observations were carried out at 1362 MHz using the Very Long Baseline Array, including the phased Very Large Array as an element. The high-resolution radio continuum images reveal a nuclear starburst region in this galaxy, which is composed of diffuse emission approximately 670 $\times$ 340 pc on the plane of the sky, and a number of compact sources. These sources are most likely to be clustered supernova remnants

[1]National Radio Astronomy Observatory, P O Box O, Socorro, NM 87801.

[2]University of Kentucky, Department of Physics and Astronomy, Lexington, KY 40506.

and/or luminous radio supernovae. Their brightness temperatures range over $(2.2\text{–}6.6)\times10^5$ K, with radio spectral luminosities between $(1-10)\times10^{21}$ W Hz^{-1}. The total VLBI flux density of the starburst region is ∼52 mJy, which is about 50% of the total flux density detected with the VLA at arcsecond resolution. For this galaxy, we derive a massive star formation rate of $\sim84\pm13$ $M_\odot$ yr^{-1}, and a supernova rate of $\sim4\pm1$ yr^{-1}. H I absorption is detected in multiple components with optical depths ranging between 0.3 and 2.5, and velocity widths between 58 and 232 km s^{-1}. The derived column densities, assuming $T_{\rm s} = 100$ K, range over $(10-26)\times10^{21}$ cm^{-2}. The H I absorption shows a strong velocity gradient of 453 km s^{-1} across 0″.36 (274 pc). Assuming Keplerian motion, the enclosed dynamical mass is about 2.3×10^9 $(\sin^{-2}i)$ $M_\odot$, comparable to the enclosed dynamical mass estimated from CO observations.

Subject headings: galaxies: individual (IRAS 17208-0014) — galaxies: starburst — radio continuum: galaxies — radio lines: galaxies — supernovae: general

1. INTRODUCTION

At luminosities above 10^{11} $L_\odot$, infrared galaxies become the most numerous objects in the local universe ($z \leq 0.3$) (Sanders & Mirabel 1996). The trigger for the intense infrared emission appears to be the strong interaction or merger of molecular gas-rich spirals. Galaxies at the highest infrared luminosities ($L_{\rm IR}(8-1000\ \mu m) \geq 10^{12} L_\odot$), known as Ultra-Luminous Infrared Galaxies (ULIRGs), appear to be advanced merger systems and may represent an important stage in the formation of quasi-stellar objects (Sanders et al. 1988).

The bulk of the energy radiated by these sources is infrared emission from warm dust grains heated by a central power source or sources. The critical question concerning these galaxies is whether the dust is heated by a nuclear starburst, or an active galactic nucleus (AGN), or a combination of both. Mid-infrared spectroscopic studies on a sample of ULIRGs by Genzel et al. (1998), suggest that 70%–80% of these galaxies are powered predominantly by recently formed massive stars, and 20%–30% by a central AGN. These authors conclude further that at least half of these ULIRGs are probably powered by both an AGN and a starburst in a 1–2 kpc diameter circumnuclear disk or ring. The most direct evidence to date of sub-kpc nuclear starburst regions in ULIRGs is the discovery of luminous radio supernovae and supernova remnants in both Arp 220 (Smith et al. 1998b) and Mrk 273 (Carilli & Taylor 2000), using VLBI observations.

In this paper, we present VLBI continuum and H I absorption observations on the

ULIRG IRAS 17208–0014 at $z = 0.0426$. This galaxy has an infrared luminosity of $L_{\rm IR} = 2.5 \times 10^{12} L_\odot$, as defined in Goldader et al. (1995).

Optical images of IRAS 17208–0014 at 6550 Å show two tidal tails from a merger (Melnick & Mirabel 1990; Murphy et al. 1996), and its optical spectrum resembles that of an H II region (Veilleux et al. 1995; Soifer et al. 2000). Its near-IR images show a very disturbed morphology and an extended but single nucleus, suggesting a complete merger (Zenner & Lenzen 1993; Murphy et al. 1996). Higher resolution near-IR images reveal numerous extremely luminous clusters in the inner 1 kpc, with no direct evidence of an AGN (Scoville et al. 2000). Infrared observations, in general, suggest that this galaxy represents the extreme of starburst dominated sources of this type (Soifer et al. 2000), and an observational proof that a collision of galaxies can lead to a mass distribution similar to elliptical galaxies (Zenner & Lenzen 1993).

The CO (1–0) emission observations of IRAS 17208–0014 by Downes & Solomon (1998) show a source of size $1\farcs8 \times 1\farcs6$ at full width half maximum, and a strong velocity gradient with a change of 400 km s^{-1} over $1\farcs5$ in position angle 120°. The enclosed dynamical mass estimated from the CO observation is $8.5 \times 10^9\ M_\odot$.

IRAS 17208–0014 also exhibits OH megamaser activity (Martin et al. 1989) at 1665, 1667, and 1720 MHz. The strongest emission is in the 1667 MHz line, with a luminosity of $L_{\rm OH} = 10^3\ L_\odot$. MERLIN 1662 MHz radio continuum observations at $0\farcs3$ resolution (Martin et al. 1989) revealed the existence of an unresolved component on the longest baselines, with a constant visibility amplitude of $\sim$35 mJy. However, the continuum emission from this galaxy was not detected in the 18 cm global VLBI observations by Diamond et al. (1999) to a limit of $3\sigma = 210\ \mu$Jy beam^{-1}.

Single dish observations by Martin et al. (1989) at Nançay showed the existence of a very wide H I absorption line in this galaxy, with full velocity widths of 650 and 695 km s^{-1} at 50% and 20% of the maximum depth, which is -12 mJy.

In this paper, we report a detailed study of the H I 21 cm absorption and the radio continuum emission from IRAS 17208–0014. The results reveal the H I gas dynamics and the distribution of compact continuum sources, possibly composed of luminous radio supernova and/or supernova remnants, in the nuclear region of this galaxy on sub-kpc scales. We adopt a distance of 171 Mpc to this galaxy, assuming $H_\circ = 75$ km s^{-1} Mpc^{-1}. At this distance 1 mas corresponds to 0.76 pc.

2. OBSERVATIONS AND DATA REDUCTION

The observations were carried out at 1362 MHz on June 4, 2001 using NRAO's [3] Very Long Baseline Array (VLBA), and the phased Very Large Array (VLA) as an element. The bandwidth of the observations was 16 MHz, in each of right and left-hand circular polarizations, sampled at two bits and centered at the frequency of the neutral hydrogen 21 cm line, at a heliocentric redshift of $z = 0.0426$, or $cz = 12790$ km s^{-1}. The data were correlated at the VLBA correlator in Socorro, NM with 512-point spectral resolution per baseband channel, and 2.6 seconds correlator integration time. The total observing time was 11 hours. An initial correlation was performed at the position reported by Diamond et al. (1999) for IRAS 17208–0014 in their 18 cm VLBI OH megamaser observations, but no emission was detected. A second and final correlation was done at the position reported by Martin et al. (1989) in their 18 cm OH megamaser and continuum observations with the VLA and MERLIN. This position, where strong fringes were detected, is about 5.5 arcseconds different from the position reported by Diamond et al. (1999).

Data reduction and analysis were performed using the Astronomical Image Processing System (AIPS) and the Astronomical Information Processing System (AIPS++). Table 1 summarizes the parameters of these observations.

Along with the target source IRAS 17208–0014, the compact source J1730+0024 was observed as a phase reference with a cycle time of 120 seconds, 80 seconds on the target source and 40 seconds on the phase reference. The source J1743–0350 was used for amplitude and bandpass calibration.

After applying *a priori* flagging and manually excising integrations affected by interference, we performed amplitude calibration using the measurements of the antenna gain and the system temperature of each station, and bandpass calibration. Different spectral averagings generated two data sets, a one-channel continuum and a 124-channel line data set. The phase calibrator J1730+0024 in the continuum data set, was self-calibrated and imaged in an iterative cycle. The self-calibration solutions of J1730+0024 were applied on both the continuum and the line data of the target source IRAS 17208–0014.

The continuum data of IRAS17208–0014 were then deconvolved and imaged with various spatial resolutions by tapering the visibility data, to reveal its continuum structure. Continuum signals were mainly detected on the short-to-moderate length baselines to the phased VLA (Y27). The H I absorption line was only detected on the shortest baselines

---

[3]The National Radio Astronomy Observatory is a facility of the National Science Foundation operated under cooperative agreement by Associated Universities, Inc.

to Y27, primarily on the Y27–Pie Town baseline. The continuum emission was subtracted from the spectral-line visibility data. The spectral-line data were then analyzed at various spatial and spectral resolutions, and imaged by applying a two dimensional Gaussian taper falling to 30% at 500 kλ. Pairs of channels were averaged together to improve the sensitivity. The resulting velocity resolution of the H I images was 58 km s^{-1}, and the spatial resolution $0\farcs55 \times 0\farcs35$. An optical-depth $\tau(\nu)$ cube was calculated from the H I absorption image cube and a continuum image with a similar resolution as $\tau(\nu) = -\ln[1 - I_{\rm line}(\nu)/I_{\rm continuum}]$. The optical depth cube was blanked in areas where the flux density of the background continuum image is below 9.4% of the peak value, i.e., less than 3 mJy beam^{-1}.

3. RESULTS AND ANALYSIS

3.1. *The Radio Continuum*

Figure 1 is our moderate resolution continuum image of the central region in IRAS 17208–0014 at 1362 MHz, with 80×63 mas (60.8×47.9 pc) resolution, obtained by using the CLEAN algorithm as implemented in the AIPS task "IMAGR", with a grid weighting intermediate between natural and uniform (ROBUST = 0). A two dimensional Gaussian taper falling to 30% at 2 Mλ in both U and V directions was applied on the visibility data. The radio continuum emission region has an extent of 670×390 pc on the plane of the sky, with a total flux density of 52 mJy. We also reduced the VLA data from these observations, which were performed in the CnB configuration and yielded a resolution of $9\farcs5 \times 4\farcs5$. The total flux density of the source at this resolution is 100 mJy, consistent with the value measured by Condon et al. (1996) at 1.425 GHz with the VLA-B array.

An important question regarding these observations is whether the extended emission is likely diffuse, or composed of many point sources as might be expected for a nuclear starburst. Due to the incomplete UV coverage in VLBI observations, especially for a source at 0° declination, the CLEAN algorithm tends to generate spurious point sources when deconvolving extended emission regions at high resolution. On the other hand, it is plausible that the extended emission is indeed composed of mostly faint point sources, in view of the likely starburst nature of IRAS 17208–0014. To resolve this ambiguity, we tested two other imaging algorithms: The Multi-Scale CLEAN and the Maximum Entropy Method (MEM), by generating two artificial data sets in AIPS++ with the same U-V sampling, weights and sky positions as our target source. Such simulations give us confidence in the reliability of the results obtained from the real observations. The first data set was composed of multiple point sources and an extended source, and the second was composed of three extended sources. While the MEM gave very poor images for the set with compact sources and relatively poor results on the set with large sources, the Multi-Scale CLEAN successfully imaged both data sets without exhibiting any tendency to generate spurious point sources. Thus, we imaged the actual observations of our target source at high resolution (Figure 2) using the Multi-Scale Clean algorithm as implemented in the AIPS++ tool "IMAGER", with a grid weighting ROBUST = 0.

Figure 2 has a resolution of 36×33 mas (27.4×25.1 pc) and represents the same region as in Figure 1. The visibility data were tapered with a Gaussian function falling to 30% at 6 Mλ in the U direction and 4.5 Mλ in the V direction. The continuum source is resolved and consists of a diffuse component extending over 670×390 pc, punctuated by a number of compact sources.

There are about 25 compact sources in this high resolution image with flux densities larger than $5\sigma = 350$ μJy beam^{-1}, but in Table 2 we list only the seven strongest compact sources, with flux densities higher than $9\sigma = 630$ μJy beam^{-1}. We selected this conservative limit because only these sources were consistently reproduced in the total intensity (Stokes I), and in the individual RR and LL images, with comparable flux densities. The remaining sources lacked this consistency.

The compact source parameters in Table 2 were obtained by fitting Gaussian functions using the tool "IMAGEFITTER" in AIPS++. The positions (Column 2) are relative to the peak surface brightness. Column 3 lists the surface brightnesses of these source, and Column 4 their integrated fluxes. Columns 5, 6 are the major and minor axes of the Gaussians at full width half maximum, and Column 7 are their position angles.

Phase-referencing observations allow the determination of the absolute position of the target source and its components, if any, from the position of the calibrator (Walker 1999). The peak emission in IRAS 17208–0014, which is 1043 μJy beam^{-1}, is found to be at α(J2000) = $17^{\rm h}23^{\rm m}21\overset{\rm s}{.}9554$, δ(J2000) = $-00^{\circ}17'00\overset{''}{.}938$. In applying the phase-referencing technique, the accuracy of the calibrator position is important. The position of J1730+0024 was obtained from the Jodrell Bank–VLA Astrometric Survey (JVAS) of phase calibrators, with a position uncertainty of $\sim$14 mas (Browne et al. 1998). We verified the reported position of this calibrator, as well as its structure and its VLBI flux density, with a short VLBA observation preceding our main observations.

3.2. *The* **H I** *Absorption*

The H I absorption detected against the whole structure of the continuum has a full width at 20% maximum of 696 km s^{-1}, and is composed of several components. Figure 3 shows Hanning smoothed spectra of H I optical depth averaged over various regions against the low resolution continuum image of IRAS 17208–0014. Figure 4 presents optical depth images covering the velocity range 13170.3–12539.0 km s^{-1}. These images explicitly show the variation of the H I opacity against the nuclear region of IRAS 17208–0014. In the lower panel of Figure 5, Figure 5*a* is the H I position-velocity (P-V) plot along the major axis of the radio source (position angle 52°), and Figure 5*b* is a P-V diagram along another cut parallel to the major axis, as shown in the continuum image at the upper panel of Figure 5. We distinguish five main absorption peaks in both the P-V and the optical-depth images. Their velocity widths range between 58 and 232 km s^{-1} at half maximum, with optical depths between 0.3 and 2.5. Table 3 summarizes the physical characteristics of these five H I absorption features. The velocities (Column 1) refer to peaks of these features as seen in the optical-depth spectra. The widths of these lines (Column 2) are the approximate full widths at half peak optical depth. $N_{\rm HI}/T_{\rm s}$ of each peak (Column 4) is calculated as $N_{\rm HI}/T_{\rm s}$ (cm^{-2} K^{-1}) = $1.823 \times 10^{18} \int \tau(v)dv$. The column densities $N_{\rm HI}$ (Column 5) are derived assuming $T_{\rm s}$ = 100 K. The visual extinction of each feature as a function of the H I spin temperature $A_{\rm v}/T_{\rm s}$ (Column 6) is computed assuming a Galactic dust-to-gas ratio (Staveley-Smith, & Davies 1987), and the visual extinctions $A_{\rm v}$ (Column 7) are also derived for $T_{\rm s}$ = 100 K.

Our analysis show that the strongest velocity gradient in the H I absorption is along a position angle of 120°, and not along the major axis of the radio source. The upper panel of Figure 6 is the H I absorption velocity field, the contours are in steps of 50 km s^{-1} and cover a velocity range between 12600 and 13000 km s^{-1}. The lower panel of Figure 6 is a P-V plot along a cut where the strongest velocity gradient is seen (position angle 120°). This gradient is 453 km s^{-1} over 360 mas (274 pc), i.e. 1653 km s^{-1} kpc^{-1}.

The spatial resolution of the low resolution continuum image and the H I images (Figures 3, 4, 5, & 6) is $0''.55 \times 0''.35$ (418 × 266 pc). The rms noise level of the H I image cube is 0.5 mJy beam^{-1}. All these images were reconstructed with natural grid weighting (ROBUST = 5 in AIPS task "IMAGR").

4. DISCUSSION

4.1. *The Radio Continuum*

At a moderate resolution (Figure 1), the nuclear region of IRAS 17208–0014 is composed of large scale structures a few hundred mas in size, with an average brightness temperature of 3×10^5 K. Our high resolution continuum results (Figure 2) show that the nuclear region is composed of a diffuse emission, covering an overall area of $0''.88 \times 0''.51$ (670×340 pc), punctuated by multiple bright compact sources with flux densities greater than five times the rms noise level, or 350 μJy. At the full resolution of our array, this region is over-resolved and does not reveal any single dominant source with very high brightness temperature. This morphology resembles those of the starburst nuclei in M 82 (Muxlow et al. 1994; Pedlar et al. 1999), NGC 253 (Ulvestad & Antonucci 1997), Arp 220 (Smith et al. 1998b), Mrk 273 (Carilli & Taylor 2000), and III Zw 35 (Pihlström et al. 2001). The average size of these compact sources is 70×48 mas (53×37 pc), and their brightness temperatures are between $(2.2\text{–}6.6)\times10^5$ K, indicating the emission is non-thermal and not from H II regions. The non-thermal emission in nuclear starburst galaxies is usually attributed to synchrotron radiation from electrons accelerated in supernova remnant shocks (Condon 1992).

4.1.1. The starburst and the star formation rate

A remarkably tight and linear correlation between the total radio continuum emission and the far-IR luminosities ($L_{\rm FIR}$) is well known in "normal" galaxies where the main energy source is not due to a supermassive black hole (Condon 1992). The most obvious interpretation of this correlation is the presence of massive stars that both provide relativistic particles via supernova events, and heat the interstellar dust which radiates in FIR wavelengths (Helou, Soifer, & Rowan-Robinson 1985; Wunderlich & Klein 1988; Condon 1992).

The ratio of infrared to radio luminosity is expressed by the quantity q as defined by Helou et al. (1985):

$$q = \log\ \{[FIR/(3.75 \times 10^{12}]/S_{1.4\ \rm GHz}\}, \tag{1}$$

where FIR is given by:

$$FIR = 1.26 \times 10^{-14}(2.58 S_{60\ \mu\rm m} + S_{100\ \mu\rm m}). \tag{2}$$

For IRAS 17208–0014, the total flux density at 1.4 GHz is 100 mJy (this work), and the IR flux densities at 60 and 100 μm are $S_{60\ \mu\rm m} = 34.67$ Jy and $S_{100\ \mu\rm m} = 37.65$ Jy, respectively (Sanders et al. 1995). The resulting q is 2.63, reasonably consistent with the mean value of 2.34 for IR selected galaxies, and dispersion of ±0.33 for galaxies with $L_{60\ \mu\rm m} > 10^{11} L_\odot$, obtained by Yun, Reddy, & Condon (2001). Values of q less than 1.64 would indicate the presence of a radio loud AGN (Yun, Reddy, & Condon 2001). Thus, based on the radio-FIR correlation, it would appear that IRAS 17208–0014 is dominated by a starburst.

An estimate of the massive star formation rate and the supernova rate for a starburst galaxy can be obtained in two independent ways. The first is a theoretical approach which assumes an initial mass function (IMF) (Scoville & Soifer 1991), and the second is based on an empirical relationship between the observed non-thermal radio flux density and the supernova rate in the Galaxy (Condon & Yin 1990).

For the theoretical approach, we assume a modified Miller-Scalo IMF of the form $\psi(M) \propto M^{-5/2}$. This function is truncated at $M_{\rm l} \leq 1\ M_\odot$ and $M_{\rm u} \geq 100\ M_\odot$ (Scalo 1986; Condon 1992; Smith, Lonsdale, & Lonsdale 1998). The models presented by Scoville & Soifer (1991) give the following relationship between the luminosity of the starburst and the star formation rate (SFR):

$$L_* = 1.18 \times 10^{10} \Big(\frac{M_{\rm l}}{1\ M_\odot}\Big)^{\alpha} \Big(\frac{M_{\rm u}}{45\ M_\odot}\Big)^{0.37} \Big(\frac{SFR}{1\ M_\odot\ {\rm yr}^{-1}}\Big) \Big(\frac{t_{\rm B}}{10^8\ {\rm yr}^{-1}}\Big)^{0.67} L_\odot, \tag{3}$$

where $M_{\rm l}$ and $M_{\rm u}$ are the lower and upper mass limits for star formation, respectively, $t_{\rm B} = 10^8$ yr is the lifetime of the starburst, and $\alpha = 0.23$ and 0.55 for $M_{\rm l} < 1\ M_\odot$ and $> 1\ M_\odot$, respectively.

The supernova rate $\nu_{\rm SN}$ of a starburst galaxy can be calculated from the star formation rate using the following expression from Smith et al. (1998b), that assumes the same IMF introduced above:

$$\nu_{\rm SN} \simeq 0.33(SFR)\frac{(M_u^{-3/2} - M_{SN}^{-3/2})}{(M_u^{-1/2} - M_l^{-1/2})} \qquad {\rm yr}^{-1}, \tag{4}$$

where $M_{\rm SN} = 8\ M_\odot$ for Type II supernovae.

To obtain the star formation and supernova rates in IRAS 17208–0014 ($L_{\rm FIR} = 2.3 \times 10^{12} L_\odot$), we use the lower and upper mass arguments obtained for Arp 220, the prototype ULIRG which has a very similar q value to our galaxy. For Arp 220 an upper limit mass was set from free-free emission and Paβ observations and the lower mass limit was set from the CO dynamical mass measurements and the adopted disk model (Smith et al. (1998b) and references therein). These limits are $M_{\rm l} = 5\ M_\odot$ and $M_{\rm u} = 28\ M_\odot$. It has also been found that the far-IR luminosity is a good measure of the bolometric luminosity produced by fairly massive ($M \geq 5 M_\odot$) young stars (Condon 1992). Thus, with these mass limits, we can state that $L_* = L_{\rm FIR}$. The resulting star formation rate (Equation 3) is $SFR \simeq 96\ M_\odot\ {\rm yr}^{-1}$, and the supernova rate (Equation 4) is $\nu_{\rm SN} \simeq 4.6\ {\rm yr}^{-1}$.

As an alternative, we can derive these rates using the empirical approach of Condon & Yin (1990), which is based on the observed Galactic non-thermal luminosity ($L_{\rm NT}$) and the supernova rate $\nu_{\rm SN}$. This relationship is

$$\Big(\frac{L_{\rm NT}}{10^{22}\ {\rm W\ Hz}^{-1}}\Big) = 13\Big(\frac{\nu}{\rm GHz}\Big)^{-\alpha}\Big(\frac{\nu_{\rm SN}}{{\rm yr}^{-1}}\Big), \tag{5}$$

where $\alpha \sim 0.8$ is the non-thermal spectral index for "normal" galaxies. Our 52 mJy total VLBI flux density for IRAS 17208–0014, which is mostly non-thermal, corresponds to a luminosity of 1.81×10^{23} W Hz^{-1}. From Equation (5), we get $\nu_{\rm SN} \simeq 1.8$ yr^{-1}, and from Equation(4) we get a massive star formation rate of 37 $M_\odot$ yr^{-1}, assuming the mass constraints as for Arp 220.

These values are lower than the rates obtained from the far-IR luminosity by a factor of 2.6, and suggest that there might be non-thermal diffuse emission which is not detected by our VLBI array. As shown by Condon (1992), the observed fraction of thermal emission in "normal" galaxies is ≤ 0.1 at 1.4 GHz. Thus, a reasonable approximation would be to consider the total VLA flux density, which is 100 mJy, to be non-thermal. Then, following the above argument with the luminosity 3.48×10^{23} W Hz^{-1} that corresponds to the detected VLA flux density, we obtain $\nu_{\rm SN} \simeq 3.4$ yr^{-1} and $SFR \simeq 71$ $M_\odot$ yr^{-1}. These values are more consistent with the rates obtained from the far-IR luminosity using similar mass limits, and support the suggestion that there is undetected diffuse flux in our VLBI observations.

We averaged the rates obtained from both the far-IR luminosity and the VLA radio flux density to obtain our best estimates for the massive star formation rate in IRAS 17208–0014, $\sim$$84 \pm 13$ $M_\odot$ yr^{-1}, and the supernova rate $\sim$$4 \pm 1$ yr^{-1}. The derived star formation and supernova rates are consistent with the rates in the ULIRG Arp 220, where Smith et al. (1998b) obtained a star formation rate of $50 - 100$ $M_\odot$ yr^{-1}, and a supernova rate of $1.75 - 3.5$ yr^{-1} in VLBI observations at 18 cm. Our supernova rate is much higher than the upper limit of 0.3 yr^{-1} that Ulvestad & Antonucci (1997) derived for the nearby starburst galaxy NGC 253 from higher-frequency VLA observations. Follow-up VLBI observations will make it possible to look for new sources (i.e. RSNe) to directly constrain both the supernova and the massive star formation rates in the nuclear starburst region of IRAS 17208–0014.

An estimate of the magnetic field strength and the pressure of the relativistic electrons responsible for the synchrotron radiation detected from the starburst region can be obtained by minimizing the summed energy in magnetic fields and relativistic particles (Miley 1980). The resulting magnetic field is $\sim$144 μGauss, and the corresponding pressure is $\sim$$6\times10^{-10}$ dyn cm^{-2}, indicating extreme physical conditions compared to the disks of spiral galaxies.

4.1.2. The nature of the compact sources

The VLBI continuum emission in IRAS 17208–0014 extends over a region of 670×340 pc, and can be explained in part by synchrotron radiation from aged supernova remnants (SNRs), but this region is also punctuated by a number of bright compact sources (Figure 2). The radio spectral luminosities of these sources range over $(1 - 10)\times10^{21}$ W Hz^{-1} at 1.362 GHz, and are at least an order of magnitude greater than the brightest radio supernovae (RSNe) seen in M 82 (Muxlow et al. 1994; Pedlar et al. 1999), but comparable to the rare class of extreme luminosity RSNe characterized by SN 1986J in NGC 891 (Rupen et al. 1987) and SN 1979C (Weiler & Sramek 2001). More recently, a substantial population of such luminous RSNe was discovered in Arp 220 by Smith et al. (1998b), who suggest that the high luminosities of those RSNe may indicate denser environments, more massive progenitors, or stronger magnetic fields relative to typical RSNe.

The compact sources revealed in our observations are a few times brighter and larger in size than the RSNe reported in the ULIRGs Arp 220 (Smith et al. 1998b) and Mrk 273 (Carilli & Taylor 2000). Thus, we presume that the compact sources in the starburst region of IRAS 17208-0014 are clustered young SNRs and/or luminous RSNe. Support for the clumpy nature of the nuclear region in IRAS 17208–0014 is provided by the high resolution near-IR images obtained with the Hubble Space Telescope NICMOS camera (Scoville et al. 2000). These images, with resolutions between $0\farcs11$ and $0\farcs22$, reveal numerous extremely luminous clusters of massive stars in the inner 1 kpc region of this galaxy.

Smith et al.(1998a) have fitted smooth Gaussian and clumped models of starburst distributions to the observed visibility functions of 11 luminous and ultra-luminous IR galaxies. Their first conclusion was that starbursts with standard RSNe are incapable of producing the radio power and structure of these galaxies. For luminous RSNe models, the Gaussian fits represented the visibility function poorly, but the clustered models, which assumed simultaneous detonation of the RSNe within one clump, were more successful. Excluding poor solutions, the sizes of these clumps ranged over 1–15 pc in diameter, and the number of supernovae per clump was between 2 and 12. These clumps are at least two times smaller than the minimum sizes implied by the Gaussian fits to our compact sources (Table 2).

However, we cannot rule out the possibility that the compact sources in our high resolution image are mainly powered by very luminous individual RSNe. Smith et al. (1998b) fit the following expression for the post-maximum light curve of luminous RSNe:

$$S_\nu = S_{\nu,\mathrm{max}}\left(\frac{\Delta t}{3\ \mathrm{yr}^{-1}}\right)^{1.3}, \tag{6}$$

where $\Delta t = t - t_o$, and $t = t_o$ is the detonation time. Following their discussion, individual RSNe will lie above our 5σ detection level for 7 years. Given our adopted supernova rate of 4 yr^{-1}, we expect to see about 28 individual luminous RSNe, in remarkable agreement with the 25 compact sources revealed in our observations.

Future multi-epoch VLBI observations would determine which of the two above assumptions better explain the nature of the compact components in IRAS 17208–0014.

4.2. *The* **H I** *Absorption*

The wide H I absorption observed against the whole extent of the nuclear region in IRAS 17208–0014, with a full width of 696 km s^{-1} at 20% maximum, is common in ULIRGs. Similar wide absorption lines have been found in Arp 220 (Mirabel & Sanders 1988), Mrk 273 (Bottinelli et al. 1985), and Mrk 231 (Dickey 1982). The present observations are consistent with the Nançay 300 m meridian telescope observations by Martin et al. (1989), who found a broad H I absorption ($\Delta V_{20\%} = 695$ km s^{-1}) centered at 12790 ± 10 km s^{-1}. The detected peak absorption flux density in our observations is -8.65 mJy, about 72% of the single dish detection.

Our observations reveal the details of the H I absorption against the radio emission in IRAS 17208–0014 (Figures 3, 4, 5, & 6). The absorption is complex, and composed of five main features (Table 3). Three of them are wide ($\Delta V_{\rm FWHM} = 174 - 232$ km s^{-1}) with $\tau < 1$, and the other two relatively narrow ($\Delta V_{\rm FWHM} = 58$ km s^{-1}) with $\tau > 1$. These two narrow lines appear to be localized features on the east edge and the north-east side of the continuum emission region (Figure 4), suggesting the existence of quiescent H I clouds in the ISM of the galaxy. The linear extent of these two features is $0.3 - 0.46$ kpc, as seen in the optical depth images (Figure 4).

The P-V diagram in position angle 120° (Figure 6-*lower panel*), shows a strong velocity gradient of 453 km s^{-1} over $0\farcs36$ (274 pc). Assuming Keplerian motion, the enclosed dynamical mass is 2.3×10^9 $(\sin^{-2} i)$ $M_\odot$, where i is the inclination angle. The rotational behavior of the H I and the derived dynamical mass are largely consistent with the results of CO $(1-0)$ emission line observations (Solomon et al. 1997; Downes & Solomon 1998). The interferometric observations of the CO $(1-0)$ by Downes & Solomon (1998) with IRAM at Plateau de Bure, show a velocity gradient of 400 km s^{-1} over $1\farcs5$ at position angle 120°, and an enclosed mass of 8.5×10^9 $M_\odot$. The resolution of these observations was $5\farcs1 \times 1\farcs6$ in position angle 47°. In both H I absorption and CO $(1-0)$ emission, the strongest velocity gradient is seen along the same direction (position angle 120°). The H I absorption results show a stronger velocity gradient (1653 km s^{-1} kpc^{-1}) comparing to the CO $(1-0)$ (346 km s^{-1} kpc^{-1}), suggesting that the H I disk represents the inner region of a larger molecular disk. A similar model was proposed for the absorbing neutral hydrogen in Mrk 231, where the observed H I disk was identified as the inner region of the molecular gas seen in CO $(1-0)$ emission (Carilli, Wrobel, & Ulvestad 1998).

It is likely that both atomic and molecular gas exist in the region where the H I absorption is detected. The emission detected in low spatial resolution (FWHM $5\farcs1 \times 1\farcs6$) CO observations arises from larger scales, and would not show variations on the scales seen in the H I absorption in IRAS 17208–0014.

The neutral hydrogen column densities of the observed absorption features are high, covering a range $(10.1 - 28.0)$ $T_s(\mathrm{K}) \times 10^{19}$ cm^{-2}. The corresponding visual extinctions A_v, assuming a Galactic dust-to-gas ratio, are between 0.066 T_s(K) and 0.174 T_s(K) mag. The discussion in Scoville et al. (1998) for Arp 220, with the infrared magnitudes obtained for IRAS 17208-0014 (Scoville et al. 2000), implies a visual extinction value of ∼22 mag, comparable to the values derived from our H I column densities with a spin temperature of T_s ∼100 K.

Our results show a very good agreement between the physical properties of the neutral H I in IRAS 17208–0014 and in the other ULIRGs previously observed in detail, namely Arp 220 (Mundell, Ferruit, & Pedlar 2001), Mrk 273 (Cole et al. 1999; Carilli & Taylor 2000) and Mrk 231 (Carilli, Wrobel, & Ulvestad 1998). The strong velocity gradients seen in the H I absorption of these galaxies suggest rapidly rotating disks which are obscuring the radio-emitting nuclear regions, while the multiple absorption features seen against different regions of the continuum indicate the existence of several discrete clouds in those disks.

5. CONCLUSIONS

We have presented the results of phase-referenced VLBI observations, using the VLBA and the phased VLA, of the 21 cm continuum emission and the H I absorption in the central ∼1.1 kpc of the very advanced merger galaxy IRAS 17208–0014.

The high resolution continuum images reveal the details of the previously undetected nuclear starburst region of this galaxy. Both diffuse and compact continuum emission are detected. The total VLBI flux is 52 mJy, and represents only half of the total flux seen with the VLA at a lower resolution, suggesting the existence of diffuse emission not detected by our VLBI array. The compact sources in the starburst region are more likely clustered luminous radio supernovae and supernova remnants, considering the H II spectra observed in this galaxy and its morphological similarities to other well-known starbursts. However, we cannot rule out the possibility that each of our compact sources is mainly powered by an individual bright RSN nested in a region that contains faded SNRs. The brightness temperatures of the compact structures seen in these observations are $> 10^5$ K. The flux density of the brightest source in the starburst region is less than 3% of the total radio flux density. The results suggest that there is no radio-loud AGN in the nuclear region of IRAS 17208–0014.

Both the far-infrared luminosity and the radio continuum flux of this galaxy imply a massive star formation rate of ∼84 $M_\odot$ yr^{-1} and supernova rate of ∼4 yr^{-1}. The estimated individual luminous RSN number agrees surprisingly well with the number of the compact sources detected above 5σ level. From the minimum energy condition, we have estimated the pressure to be $\sim 6 \times 10^{-10}$ dyn cm^{-2} and the magnetic field to be $\sim$144 μGauss in the starburst region.

The very wide H I absorption is composed of five components with velocity widths between 58 and 232 km s^{-1}. The column densities of these absorption peaks are on the order of 10^{20} $T_{\rm s}$(K), and the derived visual extinctions are between 0.066 $T_{\rm s}$(K) and 0.174 $T_{\rm s}$(K) mag. The strongest velocity gradient in the H I absorption is seen in position angle 120°, as in the CO $(1-0)$ emission. The H I position-velocity profile in this position angle shows a velocity gradient of 1653 km s^{-1} kpc^{-1}. The calculated dynamical mass, assuming Keplerian motion, is 2.3×10^9 $(\sin^{-2} i)$ $M_\odot$, comparable to the enclosed mass obtained from CO observations. The H I absorption results suggest the existence of a neutral gas disk containing several clouds, situated inside a larger scale molecular disk as seen in the interferometric CO $(1-0)$ emission line observations.

6. ACKNOWLEDGMENTS

This research has made use of the NASA/IPAC Extragalactic Database (NED) which is operated by the Jet Propulsion Laboratory, California Institute of Technology, under contract with the National Aeronautics and Space Administration. E. M. is grateful for support from NRAO through the Pre-doctoral Research Program. T. H. T. and E. M. acknowledge NSF support through grant AST 99-88341.

REFERENCES

Bottinelli, L., Fraix-Burnet, D., Gouguenheim, L., Kazes, I., Le Squeren, A. M., Patey, I., Rickard, L. J., & Turner, B. E. 1985, A&A, 151, L7

Browne, I. W. A., Patnaik, A. R., Wilkinson, P. N., & Wrobel, J. M. 1998, MNRAS, 293, 257

Carilli, C. L., Wrobel, J. M., & Ulvestad, J. S. 1998, AJ, 115, 928

Carilli, C. L., & Taylor, G. B. 2000, ApJ, 532, L95

Cole, G. H. J., Pedlar, A., Holloway, A. J., & Mundell, G. C. 1999, MNRAS, 310, 1033

Condon, J. J. 1992, ARA&A, 30, 575

Condon, J. J., & Yin, Q. F. 1990, ApJ, 357, 97

Condon, J. J., Helou, G., Sanders, D. B., & Soifer, B. T. 1996, ApJS, 103, 81

Diamond, P. J., Lonsdale, C. J., Lonsdale, C. J., & Smith, H. E. 1999, ApJ, 511, 178

Dickey, J .M. 1982, ApJ, 263, 87

Downes D., & Solomon P. M. 1998, ApJ, 507, 615

Goldader, J. D., Joseph, R. D., Doyon, R., & Sanders, D. B. 1995, ApJ, 444, 97

Helou, G., Soifer, B. T., & Rowan-Robinson, M. 1985, ApJ, 298, L7

Genzel, R., et al. 1998, ApJ, 498, 579

Melnick, J., & Mirabel, I. F. 1990, A&A, 231, L19

Martin, J. M., Bottinelli, L., Dennefeld, M., Gouguenheim, L., & Le Squeren, A. M. 1989, A&A, 208, 39

Miley, G. 1980, ARA&A, 18, 165

Mirabel, I. F., & Sanders D. B. 1988, ApJ, 335, 104

Mundell, C. G., Ferruit, P., & Pedlar, A. 2001, ApJ, 560, 168

Murphy, T. W. Jr., Armus, L., Matthews, K., Soifer, B. T., Mazzarella, J. M., Shupe, D. L., Strauss, M. A., & Neugebauer, G. 1996, AJ, 111, 1025

Muxlow, T. W. B., Pedlar, A., Wilkinson, P. N., Axon, D. J., Sanders, E. M., & de Bruyn, A. G. 1994, MNRAS, 266, 455

Pedlar, A., Muxlow, T. W. B., Garrett, M. A., Diamond, P., Wills, K. A., Wilkinson, P. N., & Alef, W. 1999, MNRAS, 307, 761

Pihlström, Y. M., Conway, J. E., Booth, R. S., Diamond, P. J., & Polatidis, A. G. 2001, A&A, 377, 413

Rupen, M. P., van Gorkom, J. H., Knapp, G. R., Gunn, J. E., & Schneider, D. P. 1987, AJ, 94, 61

Sanders, D. B., Soifer, B. T., Elias, J. H., Madore, B. F., Matthews, K., Neugebauer, G., & Scoville, N. Z. 1988, ApJ, 325, 74

Sanders, D. B., Egami, E., Lipari, S., Mirabel, I. F., & Soifer, B. T. 1995, AJ, 110, 1993

Sanders, D. B., & Mirabel, I. F. 1996, ARA&A, 34, 749

Scalo, J. 1986, Fundam. Cosmic Phys., II, 1

Scoville, N. Z., & Soifer, B. T. 1991, in Massive Stars in Starbursts, ed. C. Leitherer, N. Walborn, T. Heckman, & C. Norman (Cambridge: Cambridge Univ. Press), 233

Scoville, N. Z., et al. 1998, ApJ, 492, L107

Scoville, N. Z., Evans, A. S., Thompson, R., Rieke, M., Hines, D. C., Low, F. J., Dinshaw, N., Surace, J. A., & Armus, L. 2000, AJ, 119, 991

Smith, H. E., Lonsdale, C. J., & Lonsdale, C. J. 1998a, ApJ, 492, 137

Smith, H. E., Lonsdale, C. J., Lonsdale, C. J., & Diamond, P. J. 1998b, ApJ, 493, L17

Soifer, B. T., et al. 2000, AJ, 119, 509

Solomon, P. M., Downes, D., Radford, S. J. E., & Barrett, J. W. 1997, ApJ, 478, 144

Staveley-Smith, L., & Davies, R. D. 1987, MNRAS, 224, 953

Ulvestad, J. S., & Antonucci, R. J. 1997, ApJ, 488, 621

Veilleux, S., Kim, D.-C., Sanders, D. B., Mazzarella, J. M., & Soifer, B. T. 1995, ApJS, 98, 171

Weiler, K. W., & Sramek, R. A., 1988, ARA&A, 26, 295

Walker, C. R. 1999, in Synthesis Imaging in Radio Astronomy II, ed. G. B. Taylor, C. L. Carilli, & R. A. Perley (San Francisco: ASP), 433

Wunderlich, E., & Klein, U. 1988, A&A, 206, 47

Yun, Min S., Reddy, N. A., & Condon, J. J. 2001, ApJ, 554, 803

Zenner, S., & Lenzen, R. 1993, A&AS, 101, 363

This preprint was prepared with the AAS LaTeX macros v5.0.

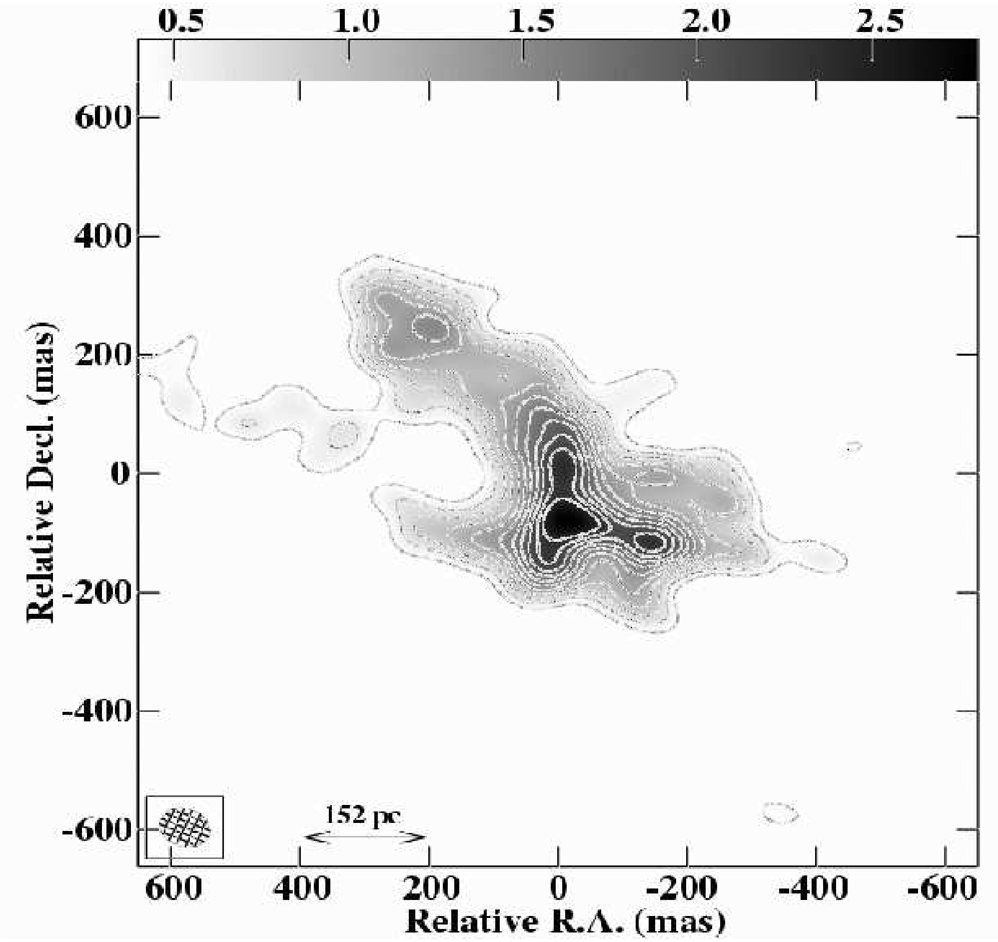

Fig. 1.— Low resolution continuum image of the central region in IRAS 17208–0014 at 1362 MHz. The restoring beam size is 80 $\times$ 63 mas in position angle 67°. The peak flux is 2.8 mJy beam^{-1}, and the contour levels are at -4, 4, 8,…24 times the rms noise level, which is 0.1 mJy beam^{-1}. The gray scale range is indicated by the wedge at the top of the image in units of mJy beam^{-1}. The reference position (0,0) is α(J2000) = $17^{\rm h}23^{\rm m}21\overset{\rm s}{.}9648$, δ(J2000) = $-00°17'00\overset{''}{.}819$. A two dimensional Gaussian taper falling to 30% at 2 Mλ was applied.

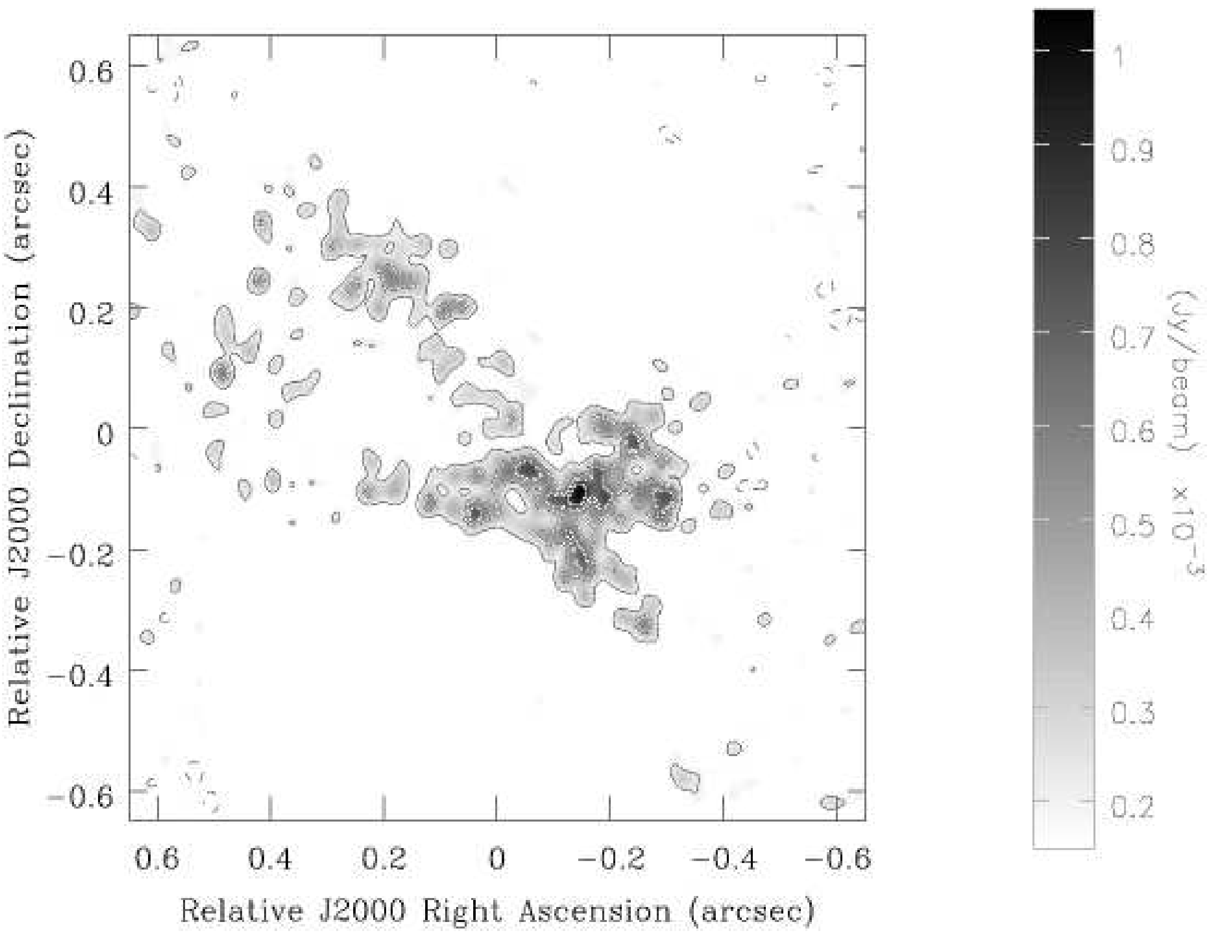

Fig. 2.— Continuum image of the central region in IRAS 17208–0014 at 1362 MHz. The restoring beam size is 36×33 mas in position angle 25°. The peak flux is 1016 μJy beam^{-1}, and the contour levels are at -3, 3, 6, 9, and 12 times the rms noise level, which is 70 μJy beam^{-1}. The gray scale range is indicated by the wedge at the right side of the image. The reference position (0,0) is α(J2000) = $17^{\rm h}23^{\rm m}21\overset{\rm s}{.}9648$, δ(J2000) = $-00°17'00\overset{''}{.}819$. A Gaussian taper falling to 30% at 6 Mλ in the U direction and 4.5 Mλ in the V direction was applied.

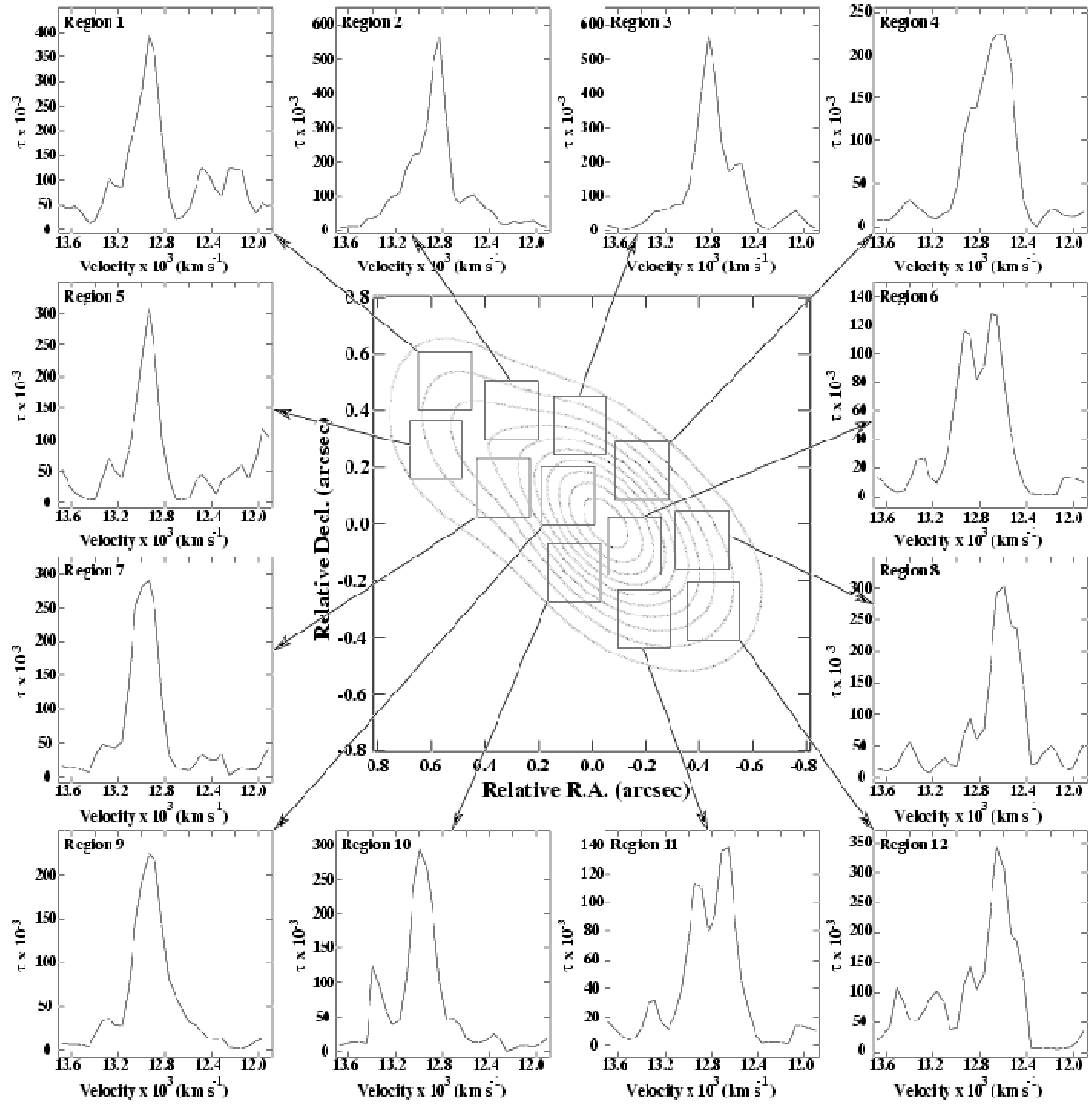

Fig. 3.— Hanning smoothed H I optical depth spectra obtained at various locations against the background continuum source IRAS 17208-0014 at 1362 MHz. All the spectra are scaled to the maximum H I absorption optical depth of each region. The restoring beam size is $0\farcs55 \times 0\farcs35$ in position angle 34°. The contour levels of the continuum image are at 3, 6,. . .30 mJy beam^{-1}, and the peak flux is 32 mJy beam^{-1}. The reference position (0,0) is $\alpha(\mathrm{J2000}) = 17^{\mathrm{h}}23^{\mathrm{m}}21\fs9648$, $\delta(\mathrm{J2000}) = -00°17'00\farcs819$.

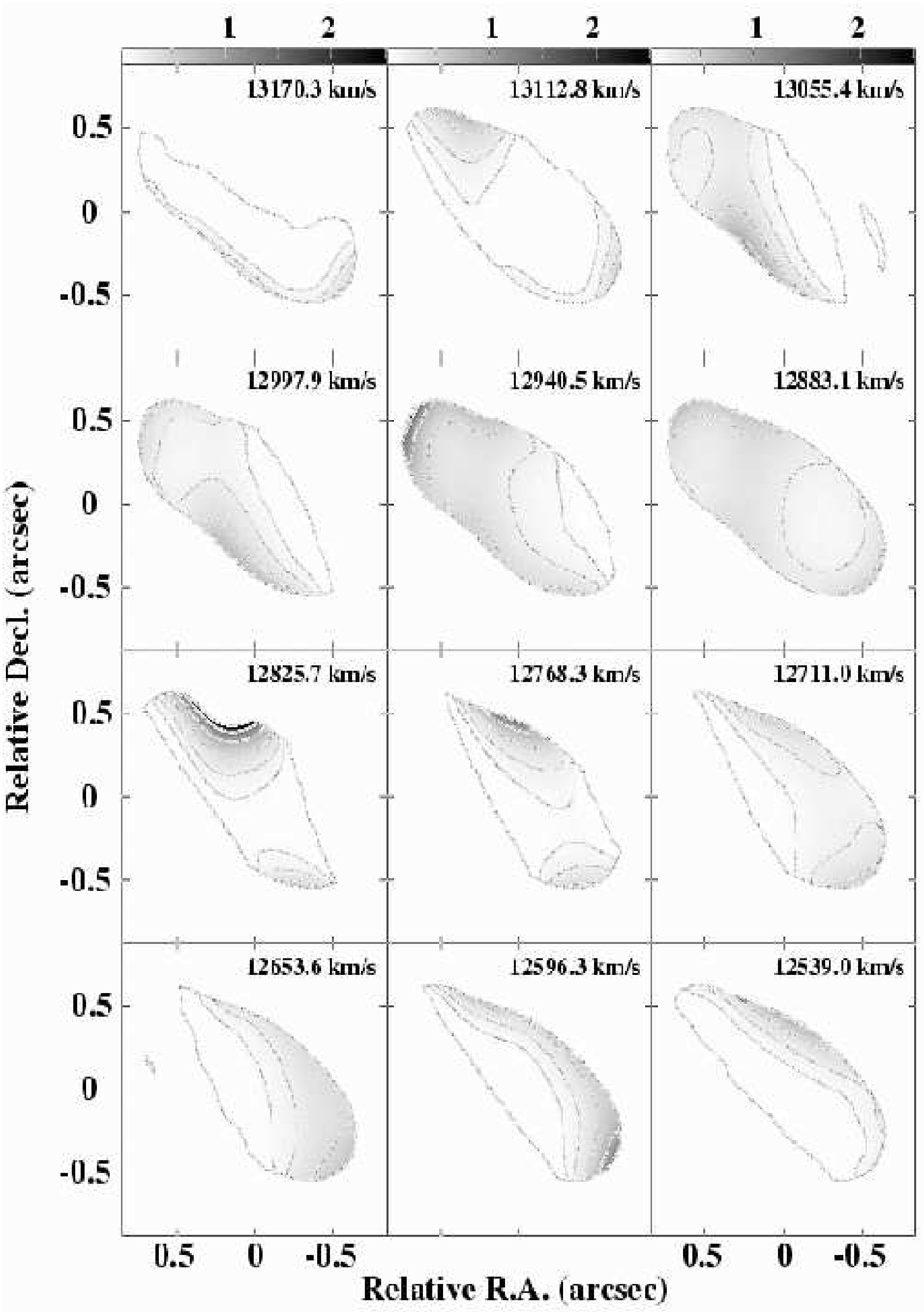

Fig. 4.— Gray-scale and contour H I optical depth channel images toward IRAS 17208–0014 in the velocity range 13170.3–12539.0 km s^{-1}. The restoring beam in these images is $0''.55 \times 0''.35$ in position angle 34°. The velocity resolution is 58 km s^{-1}. The gray-scale range is indicated by the step wedge at the top of the images; the contour levels are 0.1, 0.2, 0.4, 0.8, and 1.6.

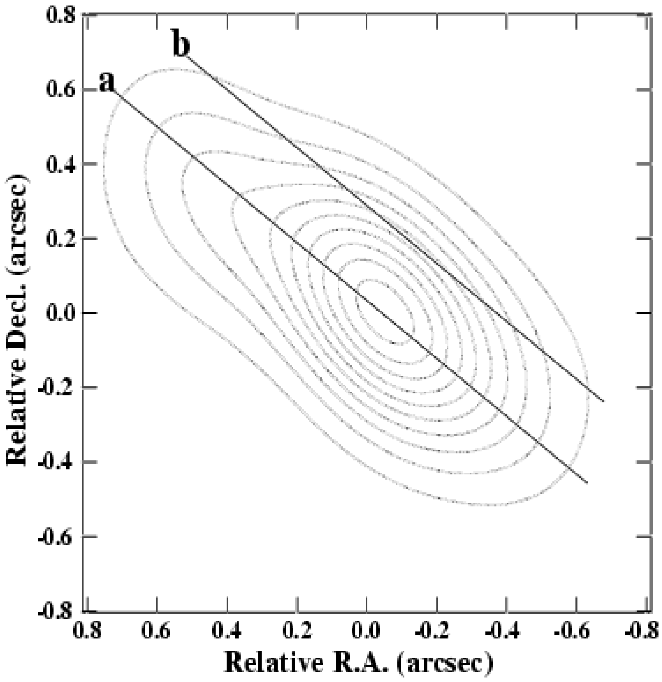

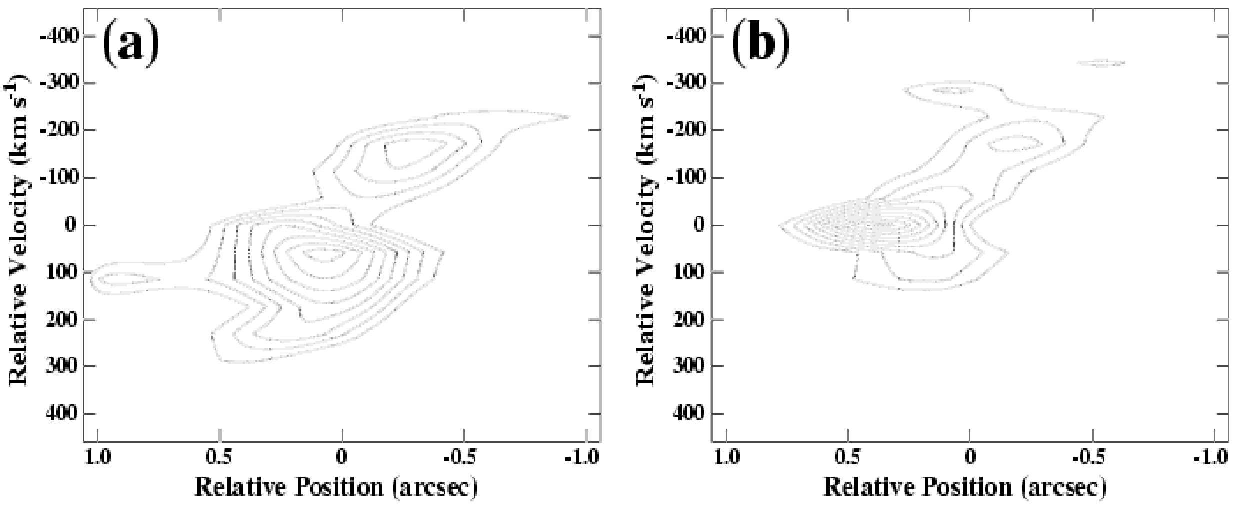

Fig. 5.— Position-velocity plots of the H I 21 cm absorption along two cuts in position angle 52°. The contour levels are at $-2, -2.5, \ldots -6$ mJy beam^{-1}. The velocity resolution is 58 km s^{-1}. The zero point on the velocity scale corresponds to a heliocentric velocity (cz) of 12825.7 km s^{-1}. The contour levels of the continuum image shown at the top are at 3, 6,…30 mJy beam^{-1}, and the peak flux is 32 mJy beam^{-1}. The reference position (0,0) is α(J2000) = $17^{\rm h}23^{\rm m}21\overset{\rm s}{.}9648$, δ(J2000) = $-00°17'00\overset{''}{.}819$. The restoring beam size is $0\overset{''}{.}55 \times 0\overset{''}{.}35$ in position angle 34°.

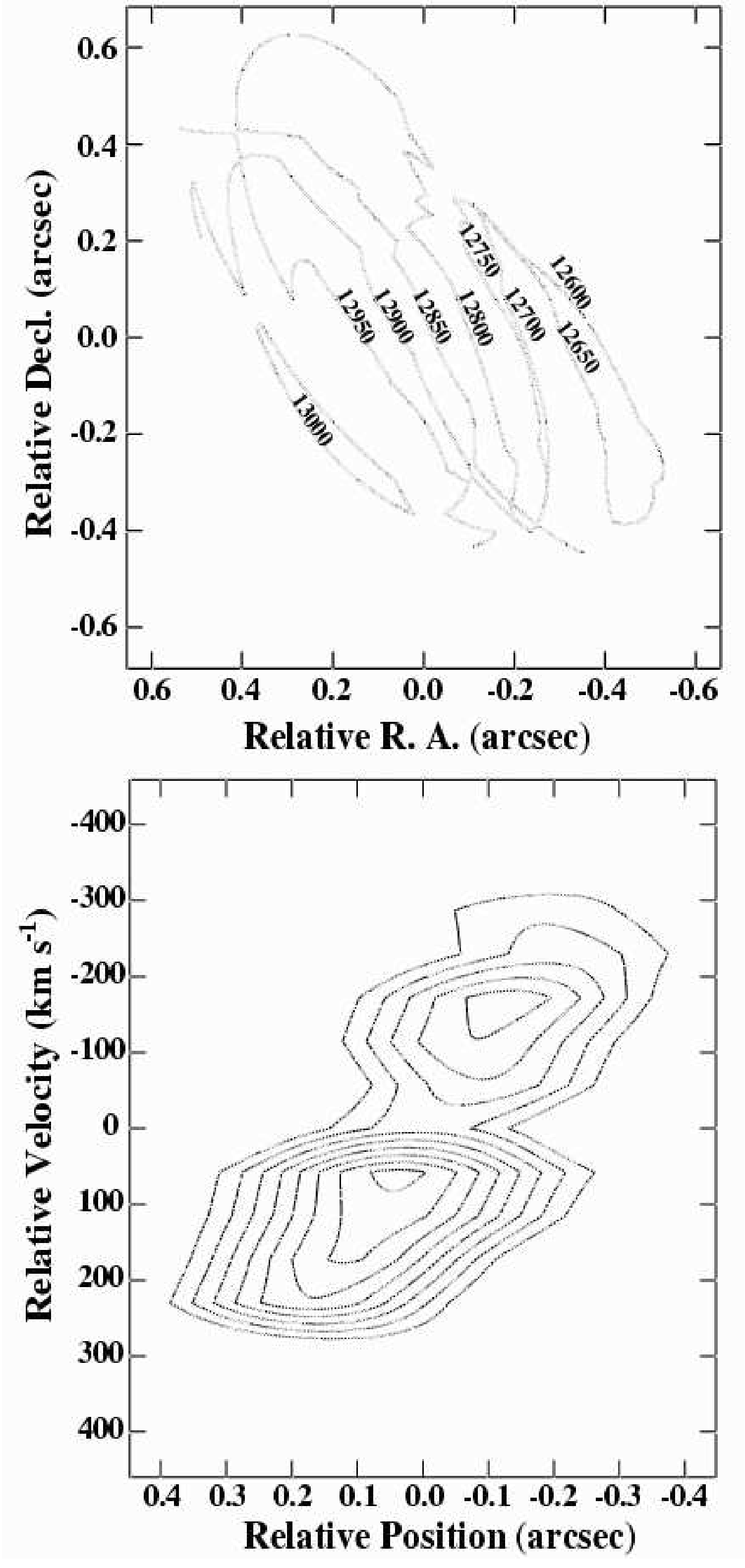

Fig. 6.— *Upper panel:* Velocity contours of the H I 21 cm absorption in steps of 50 km s^{-1}. The reference position (0,0) is α(J2000) = $17^h23^m21\overset{s}{.}9648$, δ(J2000) = $-00°17'00\overset{''}{.}819$. *Lower panel:* H I position-velocity plot in position angle 120°. The contour levels are at $-1.5, -2, \ldots -6$ mJy beam^{-1}. The zero point on the velocity scale corresponds to a heliocentric velocity (cz) of 12825.7 km s^{-1}.

Table 1. PARAMETERS OF THE VLBI OBSERVATIONS OF IRAS 17208–0014

Parameters	Values
Observing Date	2001 June 4
Observing Array	VLBA + Y27
R.A. (J2000)	17 23 21.9554
Dec. (J2000)	−00 17 00.938
Total observing time (hr)	11
Phase-referencing cycle time (min)	2
Frequency (MHz)	1362
Bandwidth (MHz)	16
Continuum image rms (μJy beam^{-1})	70
Line velocity resolution (km s^{-1})	58
Line image rms (mJy beam^{-1})	0.5
Optical depth image cutoff (mJy beam^{-1})	3

Note. — Units of right ascension are hours, minutes, and seconds, and units of declination are degrees, arcminutes, and arcseconds.

Table 2. Compact Sources in IRAS 1720–0014

Source	Relative Position[a]	Gaussian Component Parameters				
		Peak[b] (μJy beam^{-1})	Total (mJy)	Major Axis[c] (pc)	Minor Axis[c] (pc)	P.A. (°)
	(mas)					
(1)	(2)	(3)	(4)	(5)	(6)	(7)
1	0 , 0	1043.3 ± 1.0	2.764 ± 0.003	52.3 ± 0.4	34.9 ± 0.3	155
2	87E, 40N	791.1 ± 0.9	2.356 ± 0.003	50.7 ± 0.5	40.5 ± 0.4	78
3	153W, 6S	759.6 ± 1.3	2.316 ± 0.004	54.9 ± 1.3	38.3 ± 1.0	107
4	182E, 31S	737.5 ± 0.7	1.438 ± 0.001	38.5 ± 0.2	34.9 ± 0.2	122
5	98W, 86N	731.0 ± 1.0	2.269 ± 0.003	53.7 ± 1.3	39.8 ± 1.0	26
6	50W, 6S	718.7 ± 1.3	1.489 ± 0.003	45.2 ± 0.7	31.6 ± 0.2	171
7	6W, 109S	700.7 ± 2.0	2.834 ± 0.001	78.3 ± 2.0	35.6 ± 0.9	26

[a]The reference position (0,0) is $\alpha(\mathrm{J2000}) = 17^{\mathrm{h}}23^{\mathrm{m}}21\overset{\mathrm{s}}{.}9554$, $\delta(\mathrm{J2000}) = -00^\circ17'00\overset{''}{.}938$.

[b]Higher than $9\sigma = 630$ μJy.

[c]At half maximum.

Table 3. PARAMETERS OF THE H I CLOUDS

Velocity[a] (km s^{-1}) (1)	$\Delta V_{\rm FWHM}$ (km s^{-1}) (2)	$\tau_{\rm peak}$ (3)	$N_{\rm HI}/T_{\rm s}$ (cm^{-2} K^{-1}) (4)	$N_{\rm HI}$[b] (cm^{-2}) (5)	$A_{\rm v}/T_{\rm s}$[c] (mag K^{-1}) (6)	$A_{\rm v}$[b] (mag) (7)
12653.5	174	0.3	10.1×10^{19}	10.1×10^{21}	0.066	6.6
12825.7	58	2.5	28.0×10^{19}	28.0×10^{21}	0.174	17.4
12883.1	232	0.3	13.5×10^{19}	13.5×10^{21}	0.085	8.5
12940.4	58	1.3	14.4×10^{19}	14.6×10^{21}	0.094	9.4
12997.8	174	0.5	16.8×10^{19}	16.8×10^{21}	0.111	11.1

[a]Heliocentric velocity of the H I absorption feature at $\tau_{\rm peak}$.

[b]Based on $T_{\rm s} = 100$ K.

[c]Assumes a Galactic dust-to-gas ratio.